Solar and Stellar Magnetic Fields: Origins and Manifestations
Proceedings IAU Symposium No. 354, 2019
A. Kosovichev, K. Strassmeier & M. Jardine, ed.
doi:10.1017/S1743921320000095

From the Sun to solar-type stars: radial velocity, photometry, astrometry and $\log R'_{HK}$ time series for late-F to early-K old stars

Nadège Meunier and Anne-Marie Lagrange

Univ. Grenoble Alpes, CNRS, IPAG, F-38000 Grenoble, France
email: nadege.meunier@univ-grenoble-alpes.fr

Abstract. Solar simulations and observations showed that the detection of Earth twins around Sun-like stars is difficult in radial velocities with current methods techniques. The Sun has proved to be very useful to test processes, models, and analysis methods. The convective blueshift effect, dominating for the Sun, decreases towards lower mass stars, providing more suitable conditions to detect low mass planets. We describe the basic processes at work and how we extended a realistic solar model of radial velocity, photometry, astrometry and LogR′HK variability, using a coherent grid of stellar parameters covering a large range in mass and average activity levels. We present selected results concerning the impact of magnetic activity on Earth-mass planet detectability as a function of stellar type. We show how such realistic simulations can help characterizing the effect of stellar activity on RV and astrometric exoplanet detection.

Keywords. Sun: activity, Sun: faculae, plages, (Sun:) sunspots, stars: spots, stars: activity, (stars:) planetary systems, techniques: radial velocities, astrometry, techniques: photometric

1. Introduction

Our primary objective in this work is to estimate exoplanet detection limits due to stellar activity and to find new methods to correct for the stellar signal, due to magnetic activity and flows at various scales. We focus on radial velocity (RV), and compare with high-precision astrometry. This approach is necessary to be able to reach very low mass planets around solar type stars, especially in their habitable zone. The measurement of the Doppler shift is perturbed by stellar activity, for example by spots and plages which are distorting the shape of the lines (for the same reason it allows Doppler imaging or Zeeman Doppler imaging, see contributions by Solanki & Petit, this volume). To study their impact for many stellar configurations, we built synthetic time series of various observables, and in particular RV and chromospheric emission. We also generated astrometric time series to study the performance of this technique to detect low mass exoplanets, and photometric time series to evaluate the performance of various diagnosis of stellar activity for such complex activity patterns. The outline of the paper is as follows. In Sect. 1, we describe our approach, which combines our knowledge of solar activity (our reference for such stars and for which many properties are well characterized) with stellar activity and exoplanets, and our model. Results on detectability in RV and astrometry are presented in Sect. 3. We conclude in Sect. 4.

2. Approach and model

General approach. Over the last ten years, we have implemented a dedicated approach, in three steps of increasing complexity. Our original question was: could we detect the

Earth if we were observing the Sun from the outside, with current or future instruments and methods. Therefore our first step was to reconstruct the solar integrated RVs. Secondly, we developed a solar model to generate realistic structures to simulate the Sun seen from different points of view. Finally, this model was extended to the detectability of Earth mass planets in the habitable zone around solar-type stars since we were able to reproduce complex activity patterns as observed on the Sun. We describe these steps below, together with the processes taken into account when building these time series.

Step 1: Solar RV, from observed structures and MDI/SOHO Dopplergrams. We reconstructed the solar RV using observed structures (spots and plages) as well as the inhibition of the convective blueshift and a model to compute the integrated RV from these structures (Meunier *et al.* 2010a). When considering only the distorsion of the lines due to their contrasts we obtained time series with a rms (root mean square) of ∼0.3 m/s, which is very similar to what we found for spots alone (Lagrange *et al.* 2010). We found that the dominant contribution, in particular on long timescales, is the inhibition of the convective blueshift in plages, also identified early on by Saar & Donahue (1997). This process is responsible for a net redshift with a peak-to-peak amplitude of the long-term variation of 8 m/s. This is two orders of magnitude higher than the Earth signal. In addition, we confirmed this long-term variability by reconstructing the solar RV signal from MDI Dopplergrams (Scherrer *et al.* 1995), which involves no model (Meunier *et al.* 2010b). The importance of this effect was later found using other approaches, for example by Lanza *et al.* (2016) and Haywood *et al.* (2016).

Step 2: A solar model to generate spots, plages, and network. In a second step, we built a model to generate synthetic spots and plages to be able to look at different solar inclinations, and to validate this model on the Sun, before applying it to other stars. At each time step, each spot or plage is characterized by its size and its position. A contrast is then associated to each of them (it varies with the position on the disk for plages), and their lifetime is determined by a decay time following the solar distribution. Magnetic network structures are also generated from a fraction of the plage decay. The model uses several empirical laws which are well determined for the Sun. It allowed us to generate structures over complete cycles, following a given butterfly diagram and a given cycle shape, with certain size distributions, decay time distributions, and the proper dynamics. All laws are described in Borgniet *et al.* (2015). From these, we computed the RV and other observables. This allowed us to show the importance of stellar inclinations on the time series properties (Borgniet *et al.* 2015), an example is shown in Fig. 1.

Step 3: Extension of the model to solar-type stars. We built a large number of synthetic time series for stars over the range of parameters shown in Fig. 2, from F6 to K4 and for old main sequence stars (Meunier *et al.* 2019a). We adapted some of the parameters from the solar ones, but not all of them because many properties which are well known in the solar case are not well characterized for other stars, such as the size distributions for example. We also needed to keep the number of parameters reasonnable. We list in Fig. 3 the parameters which depend on spectral type, on average activity level or on both in this model. Two examples of laws are the rotation period depending on the activity level and spectral type (Mamajek *et al.* 2007), and the inhibition of the convective blueshift depending on the spectral type, which we have measured using a large sample of HARPS spectra (Meunier *et al.* 2017a, 2017b). In addition to RV time series, we also produce chromospheric emission, astrometry, and photometry time series. The latter is not presented in detail here (Meunier & Lagrange 2019c): the brightness variability, although correlated with the log R'_{HK}, exhibit a large dispersion; it increases towards low-mass stars, as observed with Kepler; The differences between brightness variability regimes dominated by spots or by plages is strongly affected by stellar inclination.

https://doi.org/10.1017/S1743921320000095 Published online by Cambridge University Press

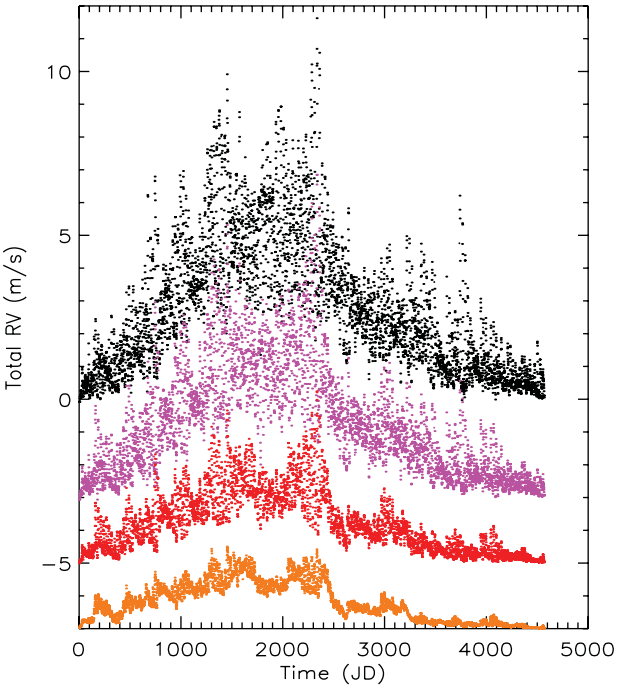

Figure 1. Solar RV from the generation of stellar spots and plages, showing the impact of inclination on short-term and long-term variability, from Borgniet *et al.* (2015).

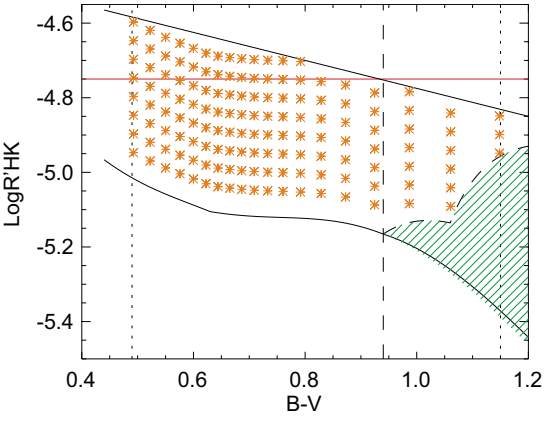

Figure 2. Range of B-V and $\log R'_{HK}$ values covered by our stellar simulations (orange stars). The upper solid line represents the transition to younger spot-dominated stars which are not modeled here (Lockwood *et al.* 2007). The lower solid line represents the basal flux (corresponding to no magnetic activity), from Meunier *et al.* (2019a).

Final sets of time series. We obtained more than 10000 independant time series of stellar structures, which are then declined in 10 inclinations and 2 spot contrasts. We also add to the RV time series granulation and supergranulation signals, using the results of Meunier *et al.* (2015). More recently, we showed that supergranulation was also affecting even long orbital periods (Meunier & Lagrange 2019a).

https://doi.org/10.1017/S1743921320000095 Published online by Cambridge University Press

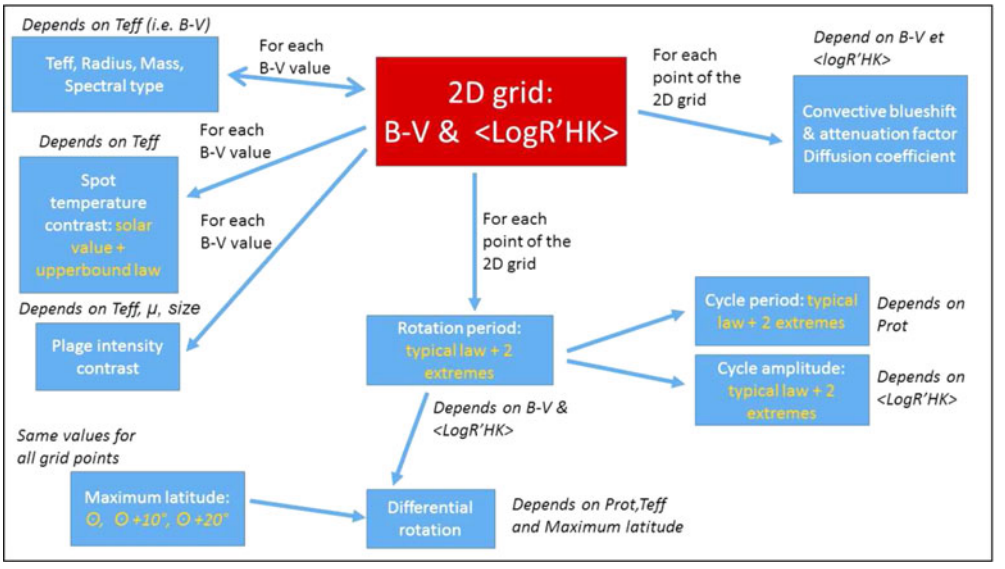

Figure 3. Parameters which are adapted in the stellar simulation and depend on B-V, on $\log R'_{HK}$, or on both, from Meunier *et al.* (2019a).

3. Results

In this section, we analyze these stellar synthetic time series. We first compute detection limits due to activity, after correction, using a simple approach. Such simulations also allowed us to better understand how stellar activity affects RV, because there are a lot of degeneracies in the final signal and many contributions from the star. We focus here on the relationship with chromospheric emission, which allows us to improve correction techniques using activity indicators. Finally, we compare our results in RV with the performance high-precision astrometry would allow to reach.

Radial velocity jitter and exoplanet detectability. As a first simple approach to study exoplanet detectability, we have estimated the mass which could be detected given the amplitude of the RV jitter after a simple correction technique, and the number of observations. For that purpose, we used a criteria established in the fitting challenge organized by Xavier Dumusque (Dumusque *et al.* 2017), in which the criterion C depending on the RV jitter, the number of observations and the planet RV amplitude was related to what we could detect given current techniques, typically ~ 7.5, was a limit between poor and good performance. The planet RV amplitude which can be detected using current correction techniques is then deduced from each time series using this criterion. Associated to a given planet orbital period (here in the habitable zone), we estimate the typical lower masses which can be detected. This is shown in Fig. 4 as a function of spectral type and $\log R'_{HK}$. With a very low number of points (100), the minimum mass is close to 10 M_{Earth}. For several 1000 points, covering full stellar cycles and an excellent sampling, values below 1 M_{Earth} can be reached, but only in a few cases: for K stars, edge-on configurations and excellent samplings. This illustrates the challenge we are facing to detect or even characterize (for example for a transit follow-up in RV) the mass of an Earth mass planet in RV in the habitable zone around such stars (Meunier & Lagrange 2019).

Limits to the usual correlation using a linear relationship between RV and $\log R'_{HK}$. A linear relationship between the long-term RV variability and $\log R'_{HK}$ is often assumed in correction techniques based on this indicator, because both are very well correlated with the plage coverage. However, this type of correction is not perfect

https://doi.org/10.1017/S1743921320000095 Published online by Cambridge University Press

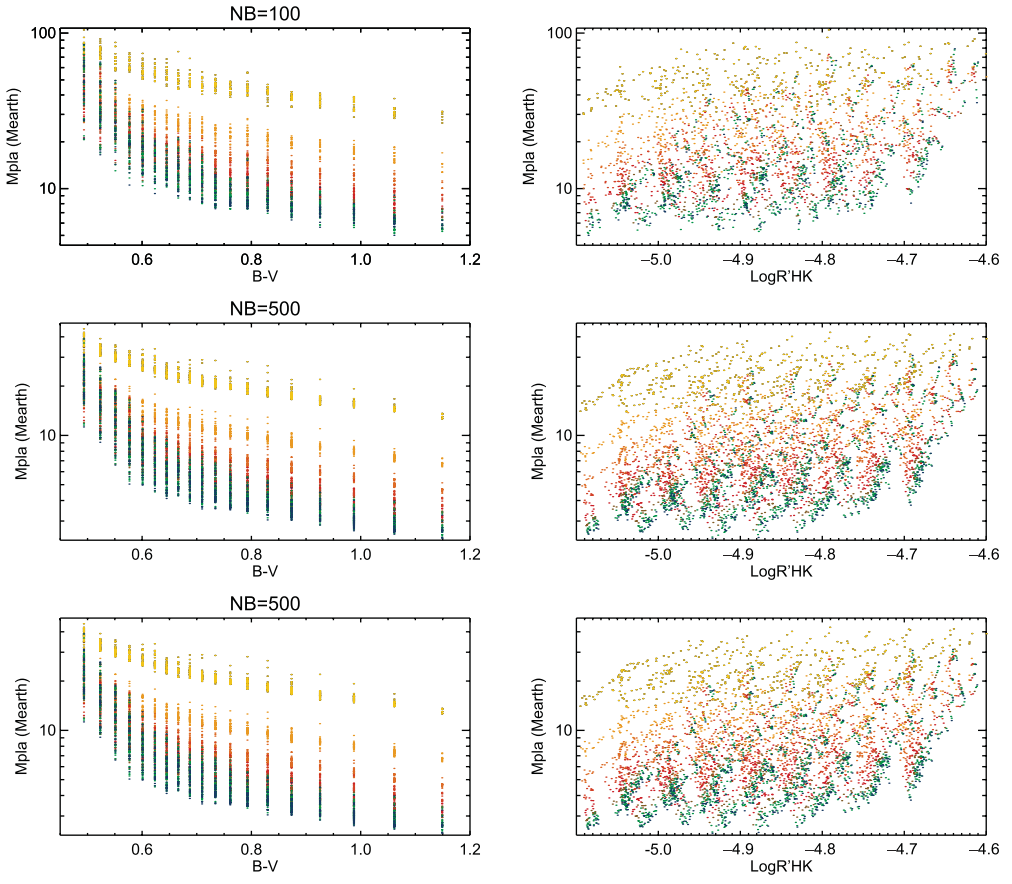

Figure 4. Lower mass which can be detected according to the criterion defined in Sect. 3 vs. B-V (left-hand side panel) and log R'_{HK} (right-hand side panel). The color code corresponds to stellar inclination, from pole-on in yellow to edge-on in green/blue, from Meunier & Lagrange (2019). Only one point out of 5 is shown for clarity.

(e.g. Meunier & Lagrange 2013). These new simulations allowed us to find out at least one important reason for this (Meunier *et al.* 2019b). Fig. 5 shows that although the chromospheric emission is roughly correlated with long-term RV as expected, there is a significant and systematic departure from a linear relationship, with difference up to 2 m/s in that example for the pole-on configuration. This example is for a star with similar activity compared to the Sun, except for the larger extent in latitude of the activity patter. Similar patterns are seen for the other simulations. The amplitude of the residuals is therefore still significantly larger than an Earth mass signal. The RV versus log R'_{HK} curves show that there is a kind of hysteresis pattern, with a different behavior between the ascending phase and the descending phase of the cycle. The sign of this pattern reverses between the two extreme configurations, with a reversal for a stellar inclination around 60°. We also observed this for the Sun and for some stars observed with HARPS. This is due to the combination of two effects: 1/ due to the butterfly diagram, the structures are not at the same distance to disk center on average over time, and the trend is reversed between pole-on and edge-on configurations; 2/ chromospheric emission and RV do not have the same dependence on the position on the disk (i.e. different projection effects). As a consequence, the ratio between the two changes over time, which leads to a departure from a linear relationship. We have

https://doi.org/10.1017/S1743921320000095 Published online by Cambridge University Press

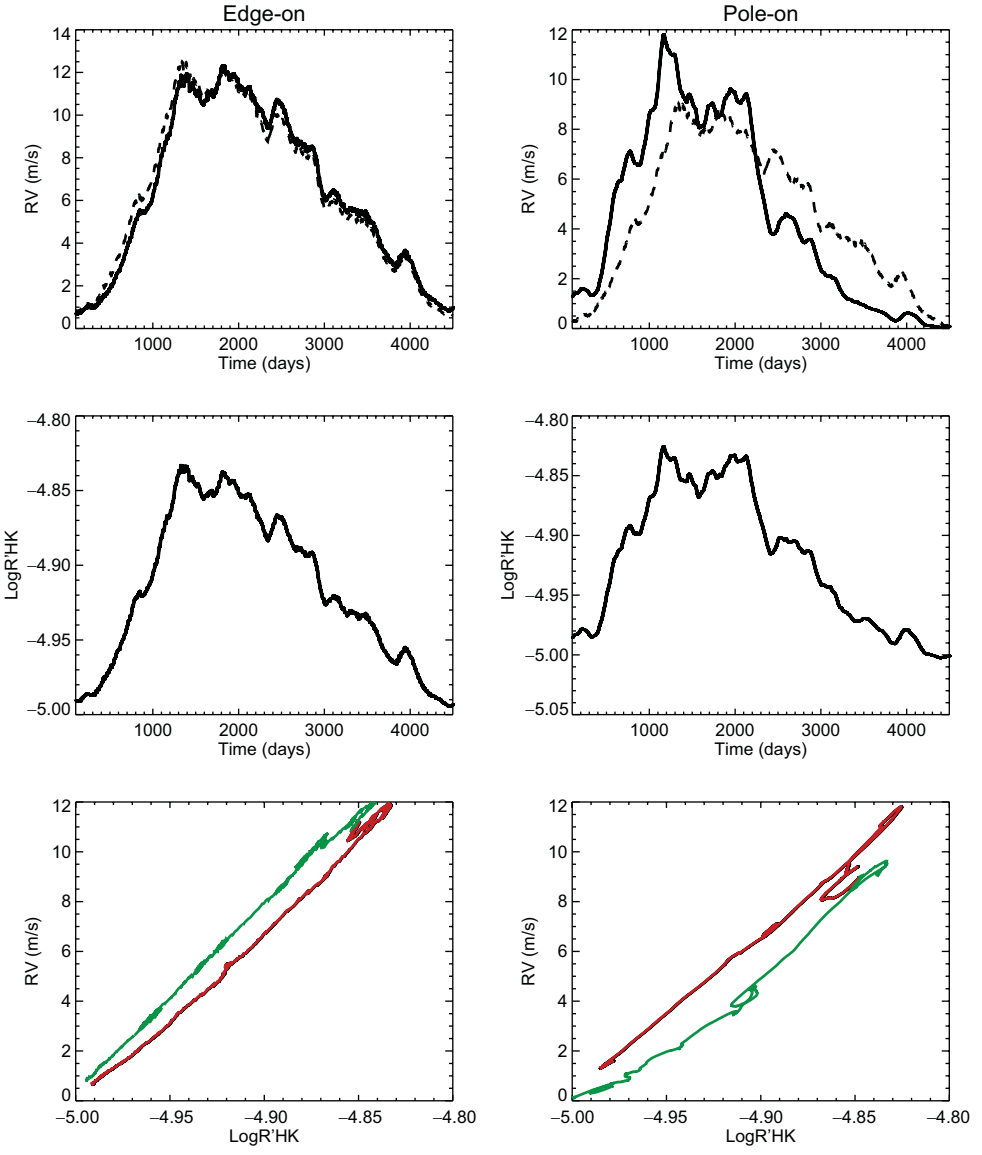

Figure 5. Example of hysteresis pattern between RV and log R'_{HK}, for the edge-on configuration (left-hand side panels) and pole-on configuration (right-hand side panels). The time series have been smoothed over 1 year to focus on long-term variability. From Meunier *et al.* (2019b).

therefore proposed a new method to take this effect into account: the correcting trend is described with functions modelling this effect for many different parameters; we choose the best function to minimize the residuals. The gains with respect to the usual linear correction are very interesting, and can reach values up to 4 or 5 in some cases (Meunier *et al.* 2019b) on the smoothed time series.

High precision astrometry. We also produce astrometric time series, corresponding to the same activity patterns. Since it is very difficult to reach very low masses with RV, it is interesting to consider the performance in astrometry, even if a mission with the necessary precision does not exist yet. For the Sun, we know this is the case: this was shown from the reconstruction of its astrometric signal over cycle 23 (Makarov *et al.* 2010;

https://doi.org/10.1017/S1743921320000095 Published online by Cambridge University Press

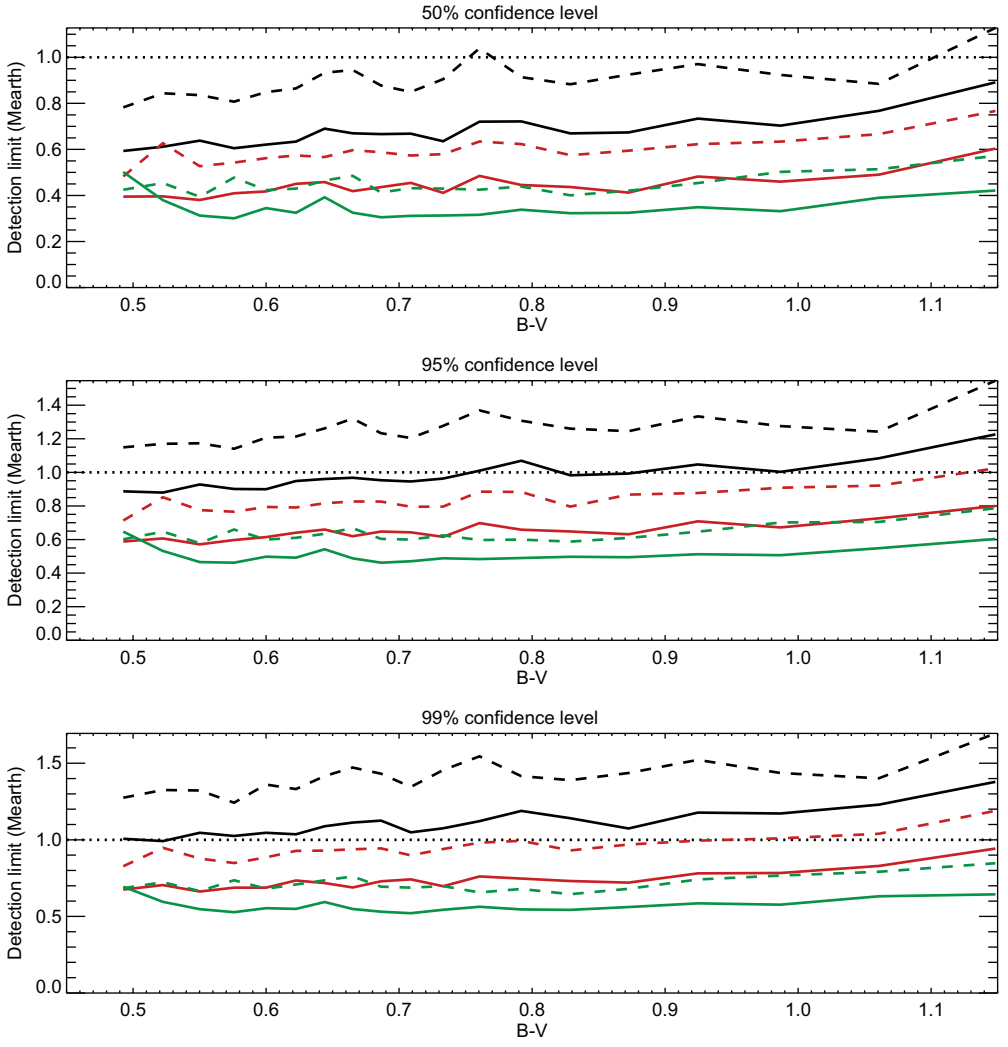

Figure 6. Detection limits in astrometry vs. B-V for different confidence levels (from top to bottom) for stars at 10 pc. The different lines correspond to different positions in the habitable zone (inner side in black, middle in red, and outer side in green) and spot contrasts (solar ones in solid lines, and upper limit in dashed lines).

Lagrange *et al.* 2011), with a typical rms of 0.07 μ as (at 10 pc) while the Earth signal at this distance would have an amplitude of 0.33 μ as so that stellar activity is not a limitation. We used the strategy proposed for the high precision Theia mission (The Theia Collaboration *et al.* 2017), i.e. 50 observations per star over 3.5 year, and 0.2 μarcsec of noise per measurement to compute detection limits on our time series (Meunier & Lagrange 2019, in prep). The detection limits for different confidence levels are shown in Fig. 6, for different positions in the habitable zone of the considered stars. We find that many of them are below 1 M_{earth}, especially for F and G stars (which are in this case slightly easier than K stars, while it was the opposite for RV). These computations were made for a star at 10 pc. The ratio between the planet signal and the stellar signal is independent on the distance. The instrumental noise is proportionnally lower for stars

https://doi.org/10.1017/S1743921320000095 Published online by Cambridge University Press

closer than 10 pc however (so we expect these detection limit to be improved) and worse for stars further away.

4. Conclusion

We showed that such realistic time series (in terms of typical amplitude and complexity of the activity pattern) are very useful to better understand the relationship between observables. Such studies have a strong impact for the exoplanet community, for both detectability and mass characterization, but also in stellar physics: for example, the hysteresis in the relationship between RV and $\log R'_{HK}$ is indicative of the sign of the dynamo wave, provided the inclination is known. This is complementary to other approaches, for example MHD simulation of granulation (Cegla *et al.* 2018), or the direct observation of solar integrated RV: many groups have indeed recently implemented dedicated instruments to be able to observe the integrated RV of the Sun as a star, for example with HARPS-N in La Palma (Dumusque *et al.* 2015; Collier Cameron *et al.* 2019), HARPS at the 3.60m in La Silla, Espress at Lowell Observatory. Based on the results obtained in the fitting challenge presented in Dumusque *et al.* (2017) and our simulations, we found that given current mitigating technique of stellar activity, Earth mass planet in the habitable zone around solar type stars is not possible, except for K stars observed in very good conditions. On the other hand, high-precision astrometry, although technically very challenging, would not be limited by stellar activity for most solar type stars (we consider old main sequence stars only in this work), at least for stars in the solar neighbourhood. Future work will include a precise determination of the detection limits we can expect from the frequential analysis of the synthetic RV time series, taking their frequential behavior into account as well as for granulation and supergranulation signals. More observables will also be added to the simulations and new correcting methods will be developed.

References

Borgniet, S., Meunier, N., & Lagrange, A.-M. 2015, *AA*, 581, A133
Cegla, H. M., Watson, C. A., Shelyag, S., Chaplin, W. J., Davies, G. R., Mathioudakis, M., Palumbo, III, M. L., Saar, S. H., & Haywood, R. D. 2018, *ApJ*, 866, 55
Collier Cameron, A., Mortier, A., Phillips, D., Dumusque, X., et al. 2019, *MNRAS*, 487, 1082
Dumusque, X., Udry, S., Lovis, C., Santos, N. C., & Monteiro, M. J. P. F. G. 2011, *AA*, 525, A140
Dumusque, X., Glenday, A., Phillips, D. F., Buchschacher, N., Collier Cameron, A., Cecconi, M., Charbonneau, D., Cosentino, R., Ghedina, A., Latham, D. W., Li, C.-H., Lodi, M., Lovis, C., Molinari, E., Pepe, F., Udry, S., Sasselov, D., Szentgyorgyi, A., Walsworth, R. 2015, *ApJL*, 814, L21
Dumusque, X. 2016, *AA*, 593, A5
Dumusque, X., Borsa, F., Damasso, M., Díaz, R. F., Gregory, P. C., et al. 2017, *AA*, 598, A133
Haywood, R. D., Collier Cameron, A., Unruh, Y. C., Lovis, C., Lanza, A. F., Llama, J., Deleuil, M., Fares, R., Gillon, M., Moutou, C., Pepe, F., Pollacco, D., Queloz, D., & Ségransan, D. 2016, *MNRAS*, 457, 3637
Lagrange, A.-M., Desort, M., & Meunier, N. 2010, *AA*, 512, A38
Lagrange, A.-M., Meunier, N., Desort, M., & Malbet, F. 2011, *AA*, 528, L9
Lanza, A. F., Molaro, P., Monaco, L., & Haywood, R. D. 2016, *AA*, 587, A103
Lockwood, G. W., Skiff, B. A., Henry, G. W., Henry, S., Radick, R. R., Baliunas, S. L., Donahue, R. A., Soon, W. 2007, *ApJS*, 171, 260
Makarov, V. V., Parker, D., & Ulrich R. K. 2010, *ApJ*, 717, 1202
Mamajek, E. A., & Hillenbrand, L. A. 2008, *ApJ*, 687, 1264
Meunier, N., Desort, M., & Lagrange, A.-M. 2010a, *AA*, 512, A39
Meunier, N., Lagrange, A.-M., & Desort, M. 2010b, *AA*, 519, A66

https://doi.org/10.1017/S1743921320000095 Published online by Cambridge University Press

Meunier, N., & Lagrange, A.-M. 2013, *AA*, 551, A101
Meunier, N., Lagrange, A.-M., Borgniet S., & Rieutord, M. 2015, *AA*, 583, A118
Meunier, N., & Lagrange, A.-M. 2019a, *AA*, 625, L6
Meunier, N., & Lagrange, A.-M. 2019, *AA*, 628, A125
Meunier, N., & Lagrange, A.-M. 2019c, *AA*, 629, A42
Meunier, N., & Lagrange, A.-M. 2019d, *In preparation*
Meunier, N., Lagrange, A.-M., Boulet, T. & Borgniet, S. 2019a, *AA*, 627, A56
Meunier, N., Lagrange, A.-M., & Cuzacq, S. 2019b, *AA*, in press
Saar, S. H., & Donahue, R. A. 1997, *ApJ*, 485, 319
Scherrer, P. H., Bogart, R. S., Bush, R. I., Hoeksema, J. T., Kosovichev, A. G., Schou, J., Rosenberg, W., Springer, L., Tarbell, T. D., Title, A., Wolfson, C. J., Zayer, I., & MDI Engineering Team 1995, *Sol. Phys.*, 162, 129
The Theia Collaboration, Boehm, C., et al. , 2017 *arXiv e-prints*, 1707.01348

Discussion

VIDOTTO: You showed a correlation between RV and $\log R'_{HK}$ when the Sun is seen edge-on, but the correlation does not hold for pole-on view. What would be the best strategy to use this correlation to other stars?

MEUNIER: The example shown in the figure was already for a star that is not the Sun, although we do see this behavior for the Sun. We have proposed a strategy to mitigate this effect by using functions describing this geometricl effect, to correct for the difference in shape between RV and $\log R'_{HK}$. In our simulations, the sign of this effect is related to the fact that we chose a solar-like butterfly diagram (equatorward dynamo wave). For a poleward pattern, the signs would be reversed. This would not change the principle of the correction method. However, if the stellar inclination of the star, it would be a novel method to determine the sign of the dynamo wave, provided it is close to pole-on or edge-on configurations to allow for a large amplitude of the hysteresis pattern.

https://doi.org/10.1017/S1743921320000095 Published online by Cambridge University Press